catalysts

MDPI

Article

Pt/Nb_2O_5-Al_2O_3 Catalysts for the Hydrogenation and Reductive Amination of Furfural

Maria H. Brijaldo [1,2,*], Hugo A. Rojas [2], Yutao Xing [3], Fabio B. Passos [4] and José J. Martínez [2]

[1] Escuela de Ciencias Administrativas y Económicas, Grupo de Investigación de Farmacia y Medio Ambiente (FARQUIMA), Universidad Pedagógica y Tecnológica de Colombia, Tunja 150001, Colombia
[2] Escuela de Ciencias Químicas, Grupo de Catálisis (GC-UPTC), Universidad Pedagógica y Tecnológica de Colombia, Tunja 150001, Colombia; hugo.rojas@uptc.edu.co (H.A.R.); jose.martinez@uptc.edu.co (J.J.M.)
[3] Instituto de Física, Universidade Federal Fluminense, Niterói 24210-346, Brazil; xy@id.uff.br
[4] Departamento de Engenharia Química e de Petróleo, Universidade Federal Fluminense, Niterói 24210-240, Brazil; fabiopassos@id.uff.br
* Correspondence: maria.brijaldo@uptc.edu.co

Abstract: Furfural is a well-recognized biomass platform. Hydrogenation and reductive amination of furfural are two principal routes in the valorization of this compound. In both reactions, the presence of reducible species (SMSI effect) and acid sites could favor the selectivity toward some interesting products. Both conditions could be obtained using metal particles supported on reducible mixed oxides. In this work, we investigate the use of Pt/Nb_2O_5-Al_2O_3 catalysts for the hydrogenation and reductive amination of furfural at distinct Nb_2O_5 contents. A decaniobate salt was used as a precursor of Nb_2O_5. The solids were reduced at 500 °C to assure the migration of reducible NbO_x species. The solids were characterized by XRD, Raman spectroscopy, HR-TEM, N_2-physisorption, NH_3-TPD and Pyr-DRIFTS. The results showed that higher Nb_2O_5 loadings led to a lower distribution of Al_2O_3 and Pt, favoring the catalysts' acidity. This fact implies that large particle size and the presence of Nb_2O_5 islands favor the formation of furfuryl alcohol but have a detrimental effect on the amine formation in the reductive amination of furfural.

Keywords: decaniobate; furfural; hydrogenation; reductive amination

Citation: Brijaldo, M.H.; Rojas, H.A.; Xing, Y.; Passos, F.B.; Martínez, J.J. Pt/Nb_2O_5-Al_2O_3 Catalysts for the Hydrogenation and Reductive Amination of Furfural. *Catalysts* **2024**, *14*, 493. https://doi.org/10.3390/catal14080493

Academic Editors: Jacek Grams and Mingyuan Zheng

Received: 30 May 2024
Revised: 23 July 2024
Accepted: 27 July 2024
Published: 31 July 2024

1. Introduction

The use of biomass has become a possible solution to the environmental problems caused by fossil fuels, which include principally pollution and the greenhouse effect. Specifically, lignocellulosic biomass is characterized as being very abundant in nature, follows the closed CO_2 cycle, and is composed of lignin, hemicellulose, and cellulose. From them, numerous compounds can be obtained that serve as platform molecules to obtain others of higher added value. An example of them is furfural [1]. Furfural (FAL) is one of the important compounds accessible from biomass, is representative of the furanic compounds, and, nowadays, is prepared from carbohydrate sources in large volume. Distinct products can be obtained from furfural by tuning reaction conditions and altering the acidity of the catalyst. Between them, the most important derivate of furfural is furfuryl alcohol (FOL) [2]. FOL is a volatile compound, has numerous applications, and is frequently employed as an intermediate in the pharmaceutical, food, and refractory industries and can be utilized as a solvent in the synthesis of polyurethane materials. Additionally, FOL can potentially be used for hydrogen storage [3].

Furfuryl alcohol is obtained through hydrogenation reaction in the gas and/or liquid phase using catalysts. Homogeneous catalysis has been used in different reaction conditions of temperature and hydrogen pressure; however, this process is characterized by the expensive separation and purification of products and high contribution to pollution of the aquatic environment [4]. Heterogeneous catalysis has the advantage that the catalysts

can be separated and reused and that it employs mild reaction conditions. Therefore, considerable attempts have been carried out to develop highly active and selective heterogeneous catalysts to transform furfural into furfuryl alcohol. Furfural has a carbonyl group and a furanic ring, which makes it a highly reactive molecule. FAL hydrogenation can produce compounds such as furfuryl alcohol, methylfuran, methyltetrahydrofuran, furan, tetrahydrofuran, cyclopentanone, or olefins [5]. However, furfural alcohol is an interesting compound due to commercial and industrial applications, as mentioned above; the scientific challenge is to reduce the carbonyl group (C=O; 171 Kcal/mol) and to maintain the furanic ring (C=C; 145 kcal/mol) intact [6,7].

Transition and noble metals, such as Cu, Ni, Co, Pd, Pt, Ir, or Ru, have been proposed as the active phase to replace the copper chromite used as a homogeneous catalyst in the industrial hydrogenation catalyst due to the high toxicity of the chromium species [8–11]. Differences in d-band width and repulsive interactions between ring and metal electrons, particle size, support acidity, and mode of activation of FAL on metal surfaces have been employed to explain the catalytic activities of distinct supported metal catalysts [9,12–14]. Pt catalysts are highly active and selective to FOL [9,12], principally due to their larger d-band width and stronger four-electron repulsive interactions between furan ring p-electrons and metal *d*-electrons, which facilitate C=O hydrogenation over Pt [13]. In addition, with an increase in Pt particle size, the (111) plane is preferentially exposed, favoring the adsorption/activation of the carbonyl group of FAL and yielding a higher amount of FOL [9,14]. Pushkarev et al. (2012) [14] found that octahedral Pt nanoparticles were selective to FOL, while cube-shaped nanoparticles produced an equal amount of furan and FOL. This behavior was attributed to the presence of two different active sites, which change in ratio with nanoparticle size and shape. The highest selectivity to FOL is achieved over 6.2 nm Pt nanoparticles with an octahedral morphology, while similarly sized 6.8 nm Pt nanoparticles with cube morphology showed a substantially lower selectivity to FOL.

Furthermore, the same metal supported on different materials could possibly give rise to different products. Especially, the acidity and basicity of the supports have a significant influence on the catalytic performance of the catalyst, particularly when alcoholic solvents are employed [15]. For example, for Pt/Nb_2O_5, the formation of corresponding acetal has been observed [6], but a change in the Lewis acid sites with W on Pt/Nb_2O_5 favored the selectivity to furan ethers [15].

Several supports have been used in furfural hydrogenation, such as metal oxides [14–17] hydrotalcites [18], and zeolites [19]. Among them, alumina (Al_2O_3) is an attractive support due to its high availability, low cost, environmental benignity, and relatively low toxicity [20,21]. Niobia (Nb_2O_5) is another support that is usually employed in conversion reactions of model biomass molecules, especially furanic derivatives [15]. It has interesting reducible properties that allow an adequate metal–support interaction as well as Lewis and Brønsted acidity, which can contribute to the formation of high-value-added chemicals, as mentioned above.

In the same way, the reductive amination of carbonyl compounds is another reaction to produce valorization of derived molecules from biomass. The reductive amination of furfural to obtain amines is an important reaction to produce surfactants, polymers, drugs, and agrochemicals [22]. This reaction takes place via two sequential reaction steps to obtain biomass amine derivates. The reaction of furfural with aniline can form (E)-1-(furan-2-yl)-N-phenylmethanimine (imine) and N-(furan-2-ylmethyl)aniline (amine). The condensation of amines with furfural leads to imines preferentially in the presence of acid catalysis. Acidic species protonate the carbonyl group, making the carbonylic carbon a better electrophile, and activates it more easily toward nucleophilic attacks [23]. In this case, an amine is the desired product, formed at the second stage of reaction (hydrogenation). Therefore, it continues to be a challenge to synthetize highly selective materials and environmentally friendly solid acids to bring about amine production. Different homogeneous and heterogeneous catalysts have been employed in this reaction [23–26]. However, the homogeneous catalysts sometimes show difficulty being separated from the reaction system or generate

pollution. Heterogeneous catalysts can improve the reductive amination showing high yields, with the advantage of easy separation. The selectivity strongly depends on the metal employed and on the hydrogenation step of imine intermediates. Our research group studied the reductive amination of furfural over Pt, Ir, and Au supported on sulfonic acid-functionalized silica (SiO_2–SO_3H) [23]. The interaction of SO_3H sites favored the formation of imine and its subsequent hydrogenation to amine, making it possible to control the yield to amine with ethyl acetate. The order of activity in the reductive amination of furfural with aniline was Pt ≈ Ir >Au [24].

Recently, the reductive amination of other aldehydes has also been studied. For example, Dong et al. [22] explored the selective reductive amination of furfural to furfurylamine with ammonia over Ru/HZSM-5 catalysts. They found that the incorporation of rhodium species into HZSM-5 had an important increase in the acid sites of the Ru/HZSM-5 catalyst. The increase in strong acid sites may be related to the interface RuO_2 forming by the strong interaction between Ru and Al, which is more obvious as the aluminum content increases. The Ru/HZSM-5(46) (SiO_2/Al_2O_3 = 46) system with optimized acid sites and Ru-O-Al bond interaction exhibited a great catalytic performance, producing a 76% yield of furfurylamine at only 15 min [22]. Ru nanoparticles have been used for reductive amination of various carbonyl compounds, and the flat morphology and surface electrons provided to the catalytic performance [27].

On the other hand, furfuryl alcohol has also been a feedstock to production of furfurylamine using Raney Ni systems [28]. However, there are very few studies about the furfural amination due to easy hydrogenation of the carbonyl group and the ring-opening reaction. Nakamura et al. [29] showed that Lewis acid sites on Pt-supported catalysts promoted the formation of amine for the amination of ketones. In the same way, Liang et al. [30] found that RuO_2 with strong Lewis acid sites favors the activation of the carbonyl group, while metallic Ru contributes to the transformation of imine to amines. Therefore, control of acid sites on metal-supported catalysts leads to an efficient role for reductive amination of carbonyl compounds. However, studies that relate the catalyst acidity and reductive amination behavior are still scarce.

Considering the above results, in this research, we prepared Pt catalysts supported on Nb_2O_5, Al_2O_3, and Nb_2O_5/Al_2O_3. Pt catalysts containing Nb_2O_5 should be adequate catalysts in the reductive amination as in the hydrogenation of furfural. Nb_2O_5 presents both Brønsted and Lewis acid sites, and its surface acidity can be changed with the calcination temperature [31] or the deposition of Nb_2O_5 over other metallic oxides as Al_2O_3, where it is possible to increase material acidity with niobia loading on Al_2O_3 [32].

Mixed oxides generally showed a better catalytic behavior than those supported on simple oxides [33], possibly due to the coverage of MeO_x species on the metallic particles or by an increase in the acidity surface. This way, these types of solids are useful in hydrogenation or reductive amination processes of renewable raw materials, because the acidity surface and decoration effect of NbO_x species could modify the selectivity of the reaction.

Commonly, the deposition of NbO_x species on Al_2O_3 is performed by impregnation with niobium oxalate [15,32] or $NbCl_5$ [34]. Polyoxometalates (POMs) as decaniobate ion ($[Nb_{10}O_{28}]^{6-}$), where the more representative compound is $TMA_6[Nb_{10}O_{28}]$, (TMA+: tetramethyl ammonium ion) can also serve as precursors to obtain mixed oxides. However, the use of these solids as catalysts or as precursor catalytics is scarce. Our recent interest has demonstrated that this type of POMs has a broad application in organic synthesis [35]. In this work, we studied the furfural hydrogenation to furfuryl alcohol production and reductive amination of furfural under mild reaction conditions using Pt on Nb_2O_5/Al_2O_3 supports. In addition, decaniobate salt was used as a precursor of Nb_2O_5, and Nb_2O_5 loading was varied (0%, 1%, 10%, and 20% (*w*/*w*)).

2. Results and Discussion

2.1. Catalyst Characterization

The XRD diffractograms of supported platinum catalysts are shown in Figure 1. The signal characteristics of the supports were evidenced for Pt/Nb_2O_5 and Pt/Al_2O_3 diffractograms, being TT-Nb_2O_5 (pseudo hexagonal) (JCPDS: 28-317 umeshbabu2017.pdf) and γ-Al_2O_3 (JCPDS 00-050-0741), respectively. For mixed oxides, only the $Pt/Nb_2O_5(25)/Al_2O_3$ diffractogram showed reflections associated with TT-Nb_2O_5. That accounts firstly for the good dispersion of the niobia for loading lower than 10% and secondly for the fact that the impregnation of decaniobate precursor induced no agglomeration. The average crystallite size of Nb_2O_5 was calculated by the Scherrer equation [36] using reflections of the TT-Nb_2O_5 phase from the XRD data of the Pt/Nb_2O_5 and $Pt/Nb_2O_5(25)/Al_2O_3$ systems, which resulted in a similar size of around 17.0 nm and 18.1 nm, respectively, which is in accordance with some studies carried out where it is indicated that the crystallite size of Nb_2O_5 is between 5 nm and 30 nm [37–39]. The above values can be related to the calcination temperature, which was 550 °C. The intensity of the Pt (111) signal at 39° near the reflection at 39.22 (222) of γ-Al_2O_3 is associated with metal crystallites that grow as the niobia content increases. This signal was more evident in the case of $Pt/Nb_2O_5(10)/Al_2O_3$ and $Pt/Nb_2O_5(25)/Al_2O_3$.

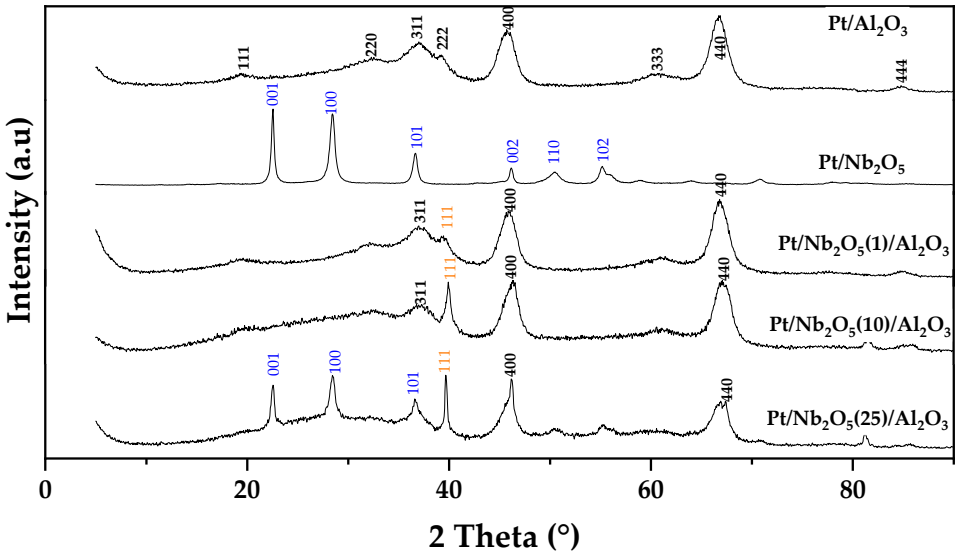

Figure 1. XRD diffractograms of supported platinum catalysts.

Figure 2 displays the Raman spectra in the region of 100~1100 cm^{-1}. Pt/Nb_2O_5 exhibited bands at 110 and 225 cm^{-1} related to the Nb-O-Nb stretch, and a band at 680 cm^{-1} attributed to the stretching Nb-O [37]. However, the Pt/Nb_2O_5 (25)/Al_2O_3 catalyst showed the above-mentioned bands but they were of lower intensity. In this system, a band at 932 cm^{-1} was also detected, which may be attributed to terminal Nb=O bonds within different isolated or polymerized NbO_x surface species [1]. In this same way, Pt catalysts supported on mixed oxides $Nb_2O_5(1)/Al_2O_3$ and $Nb_2O_5(10)/Al_2O_3$ exhibited only a weak and small band of around 150 cm^{-1}, indicating a scarce Nb-O-Nb stretch. This behavior is in agreement with the DRX results, where the $Pt/Nb_2O_5(1)/Al_2O_3$ and $Pt/Nb_2O_5(10)/Al_2O_3$ did not show diffraction peaks related to the presence of niobia, suggesting a good distribution of Nb_2O_5 species on the alumina surface or poor crystallinity [40], principally for the solid that contains 1% and 10% of Nb_2O_5. The $Pt/\gamma\text{-}Al_2O_3$ catalyst has not shown Raman bands due to the low polarizability of light atoms and the ionic character of Al–O bonds [41].

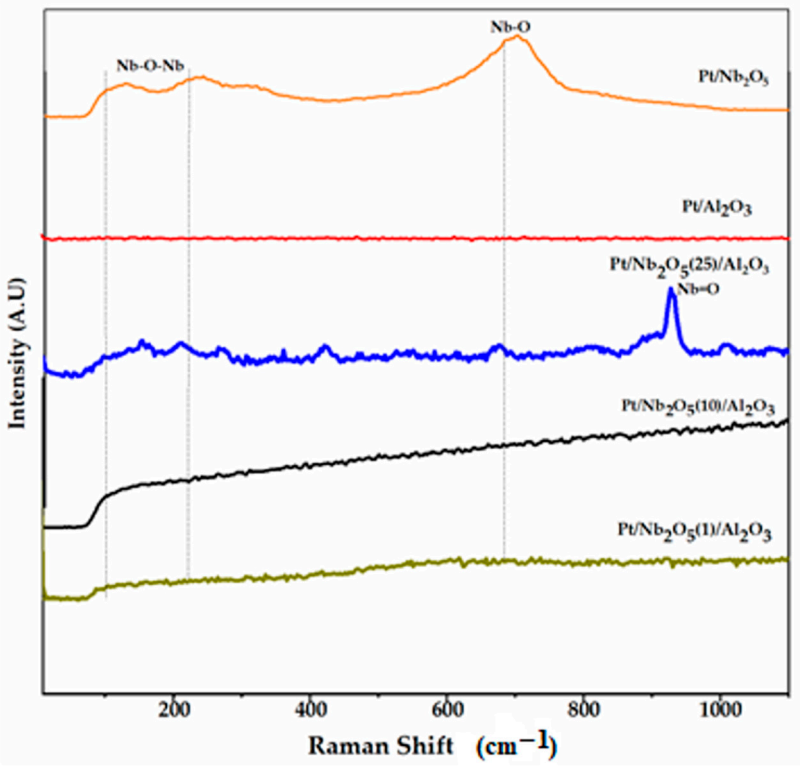

Figure 2. Raman spectra of supported platinum catalysts.

Textural properties of catalysts obtained from nitrogen sorption at −196 °C are displayed in Figure 3. It can be seen that Pt/Nb_2O_5 exhibited a type V isotherm with H3 hysteresis, and the isotherms for catalysts containing Al_2O_3 are assigned to type IV with H2 hysteresis, which indicates 'ink bottle'-type pores, according to the IUPAC classification. The deposition of niobia on the alumina surface has not altered the type of isotherm, which could be related with the uniform deposition of niobia on the alumina surface. The differences in the surface area and pore diameter shown in Table 1 could be due to blockage of alumina pores by niobia in Pt/Nb_2O_5 (1)/Al_2O_3 and Pt/Nb_2O_5 (10)/Al_2O_3 systems. However, the Pt/Nb_2O_5 (25)/Al_2O_3 catalysts showed an increase in surface area (214 m^2/g) compared with the Pt/Al_2O_3 system (196 m^2/g). This behavior may be related to the formation of new mesoporosity due to an increase in Nb_2O_5 content (25%), which was reflected by the presence of pore sizes of 4.7, 6.9, and 9.6 nm in the Pt/Nb_2O_5 (25)/Al_2O_3 catalysts. Figure S1 shows the pore size distribution to platinum-supported catalysts by BJH adsorption.

The dispersion of the metal on the support was determined by hydrogen chemisorption, and the results are presented in Table 1. The greater dispersion was found for the Pt/Al_2O_3 catalyst with 59%, while the Pt/Nb_2O_5 system presented the lowest dispersion of the active phase (37%). The low dispersion of the Pt/Nb_2O_5 catalyst may be associated with the surface area, since having a lower surface area, it is possible that the platinum particles are not well-dispersed. Regarding the systems enriched with niobia ($Pt/Nb_2O_5/Al_2O_3$), it was observed that, as the Nb_2O_5 content increased, the dispersion of platinum decreased from 54% to 45%. For the $Pt/Nb_2O_5(1)/Al_2O_3$ and $Pt/Nb_2O_5(10)/Al_2O_3$ systems, this behavior can be related to the decrease in the surface area. However, for the $Pt/Nb_2O_5(25)/Al_2O_3$ catalyst, this fact does not apply and may be related to other factors such as the isoelectric point of the support.

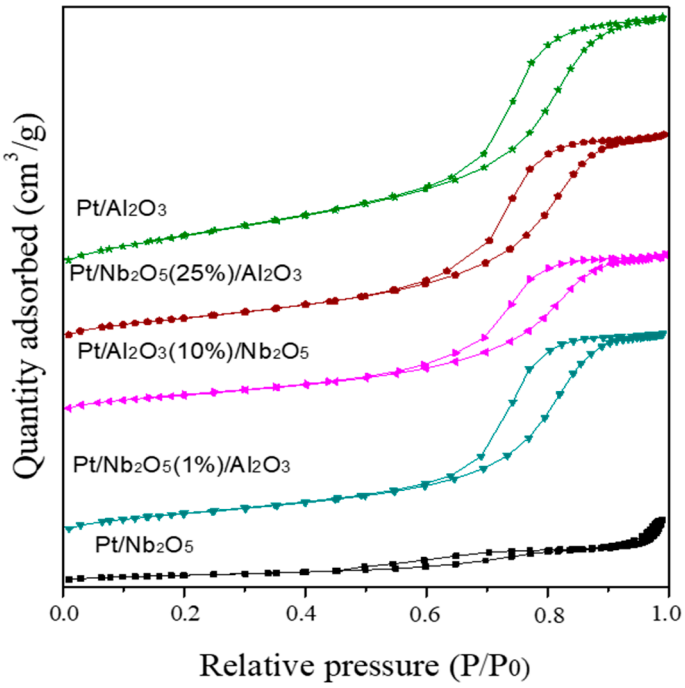

Figure 3. Nitrogen adsorption–desorption isotherms for the supported platinum catalysts.

Table 1. Textural properties and particle size of Pt catalysts.

Catalyst	S_{BET} (m^2/g)	Pore Diameter (nm)	Particle Size [a] (nm)	Dispersion [b] (%)
Pt/Al_2O_3	196	7.4	1.8	59
Pt/Nb_2O_5	55	10.4	3.5	37
$Pt/Nb_2O_5(1)/Al_2O_3$	175	9.8	5.8	54
$Pt/Nb_2O_5(10)/Al_2O_3$	157	8.6	7.3	48
$Pt/Nb_2O_5(25)/Al_2O_3$	214	7.6	8.0	45

[a] Calculated by TEM; [b] Calculated by H_2-chemisorption.

In the case of the $Pt/Nb_2O_5(25)/Al_2O_3$ system, although it exhibited the largest surface area (213 m^2/g), the particle size was the largest of all the systems. This fact may be related to the isoelectric point of the support. Alumina and niobia have isoelectric points of 8.6 and 4.0, respectively. It is known that the surface of the supports above the isoelectric point becomes negatively charged and the surface below becomes positively charged. Additionally, and taking into account the anionic nature of the precursor of the active phase (H_2PtCl_6) [42,43] it is possible that, when carrying out a high enrichment of niobia (25%) to the alumina, the Pt particles agglomerate, causing a larger particle size and lower dispersion without having an influence on the high surface area of the support.

Figure 4 shows the results of temperature-programmed desorption of NH_3. The strength of acid sites depends on the temperature in which the desorption peaks of NH_3 appear. It has been accepted that the order of acidity strength is as follows: weak (<150 °C), medium (150 and 400 °C), and strong (>400 °C). Under these criteria, it can be seen, in Figure 4, that the intensity of intermediate acid sites decreases with the loading of Nb_2O_5 on Al_2O_3; this fact is observed clearly for $Pt/Nb_2O_5(10)/Al_2O_3$ and $Pt/Nb_2O_5(25)/Al_2O_3$. However, for the latter, there was an increase in the strong acid sites. Previously, Rodrigues et al. [32] assumed that the increase in the acidity is related to the niobia content due to the formation of niobia islands on the alumina surface. Similar results could be assumed in this work, because the solid with a higher total acidity has the highest content of Nb_2O_5 (Table 2).

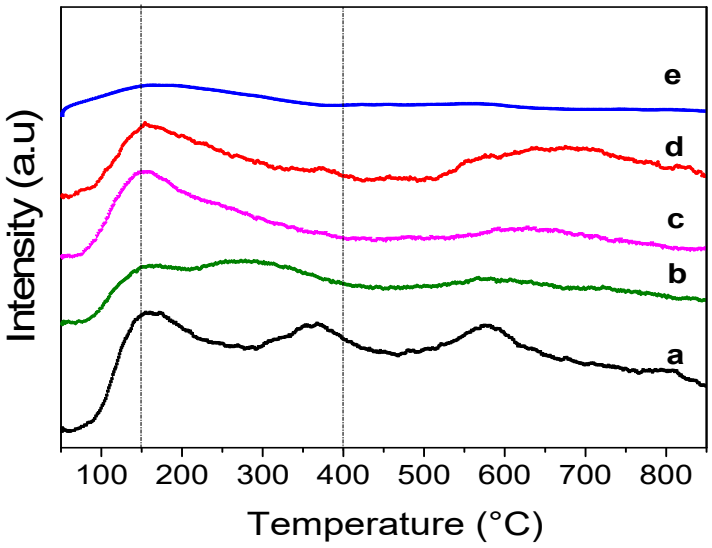

Figure 4. TPD-NH_3 of supported platinum catalysts, where (a) Pt/Al_2O_3; (b) $Pt/Nb_2O_5(1)/Al_2O_3$; (c) $Pt/Nb_2O_5(10)/Al_2O_3$; (d) $Pt/Nb_2O_5(25)/Al_2O_3$; (e) Pt/Nb_2O_5.

Table 2. Surface atomic ratios and total acidity of Pt catalysts supported.

Catalyst	Pt/(Nb+Al) [a]	Nb/Al [a]	Total Acidity (mol_{NH_3}/g cat.)
Pt/Al_2O_3	0.001	–	0.14
Pt/Nb_2O_5	0.001	0.0039	0.03
$Pt/Nb_2O_5(1)/Al_2O_3$	0.0023	0.0170	0.52
$Pt/Nb_2O_5(10)/Al_2O_3$	0.0067	0.0232	0.77
$Pt/Nb_2O_5(25)/Al_2O_3$	0.0041	–	1.03

[a] Atomic ratio Pt/(Nb+Al) and Nb/Al derived from XPS peak areas.

Pyridine adsorption spectra are shown Figure 5. The bands at 1577 and 1445 cm^{-1} appeared for all catalysts, and those are related to coordinately bonded pyridine adsorbed on Lewis acid sites (L). The small bands at 1540 and 1637 cm^{-1} are related to Brønsted acid sites (B). These bands also were weakly detected for $Pt/Nb_2O_5/Al_2O_3$ solids. The co-adsorption on Lewis and Brønsted sites was observed at 1490 cm^{-1}, being of low intensity for all systems of mixed oxides. Significant band shifts and generation of Brønsted acid sites were not observed, contrary to that reported by Rodrigues et al. [32], where they assumed that deposition of niobia on the alumina surface generates new Brönsted sites. In consequence, our results reveal that, for $Pt/Nb_2O_5/Al_2O_3$, the acidity is preferentially of the Lewis type, and increases due to the strong acid sites preferentially formed of niobia islands on the alumina surface.

Figure 6 shows representative TEM images and the corresponding particle size distribution histograms of Pt catalysts reduced at 500 °C. In these images, the platinum particles are highlighted as the darkest pseudospheres. To identify the particles of platinum and oxides of niobium and aluminum, scanning transmission electron microscopy (STEM) in combination with energy-dispersive X-ray (EDX) was carried out. The EDX maps indicate the presence of particles of platinum, aluminum in large amounts, and a high dispersion of niobium in the system; however, the niobium oxide could not be clearly differentiated from aluminum oxide using TEM and STEM-EDX techniques. An example is shown below for the $Pt/Nb_2O_5(1)/Al_2O_3$ catalyst in the Supplementary Material (Figure S2). The particle size distribution histograms exhibit platinum particle sizes between 1 and 18 nm for the mixed oxide catalysts, showing a low frequency for particles of 12–18 nm.

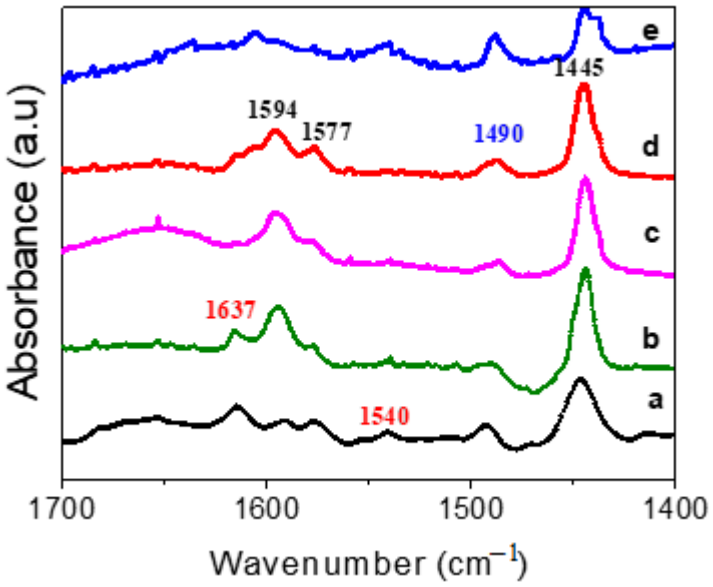

Figure 5. Pyridine adsorption spectra of supported platinum catalysts, where (a) Pt/Al_2O_3; (b) $Pt/Nb_2O_5(1)/Al_2O_3$; (c) $Pt/Nb_2O_5(10)/Al_2O_3$; (d) $Pt/Nb_2O_5(25)/Al_2O_3$; (e) Pt/Nb_2O_5.

The particle size distribution histogram of the Pt/Al_2O_3 catalyst indicates that the largest number of particles exhibit sizes of 1 to 2 nm. The average diameter of the Pt particles was found to be 1.8 nm for this catalyst, being the lowest particle size compared with the other solids. The deposition of metal on Nb_2O_5/Al_2O_3 leads to an increase in the particle size of platinum. It is possible that, with the increase in the niobia content on the alumina, there is a decrease in the isoelectric point of the mixed oxides. Thus, with a higher content of niobia (25%), the surface is possibly going to have a greater range of negative charges during the impregnation step. As the precursor of Pt is anionic in solution, it tends to agglomerate on the surface, and this could be the reason for the increase in Pt particle size observed for the mixed oxides.

Figure 7 shows the SEM-EDX micrographs of the $Pt/Nb_2O_5(25)/Al_2O_3$ catalyst and the mapping images, indicating a non-uniform distribution of niobio (orange) on alumina (green). This niobia distribution is similar to islands. SEM-EDX techniques did not allow the identification of platinum particles.

Surface species of the passivated catalysts were analyzed by XPS (Figure 8). In the region of Pt 4f for Pt/Nb_2O_5 catalyst there were peaks at 71.2 eV and 74.9 eV, which are related to the presence of Pt^0 and Pt^{2+} from PtO_x species [44]. However, these peaks were overlapped with the presence of the Al 2p peak, in the case of the Pt/Al_2O_3 catalyst, hampering a correct determination of the Pt oxidation state. In the case of platinum supported on Nb_2O_5/Al_2O_3 systems, a small contribution at 70.5 eV was also seen, indicating Pt^0 species. The peak $4f_{7/2}$ increased with Nb_2O_5 content in mixed oxides, being more evident in the case of $Pt/Nb_2O_5(10)/Al_2O_3$, suggesting a greater contribution of Pt species in this catalyst. In the region Nb 3d, Pt/Nb_2O_5 catalyst XPS showed binding energy values at 207.6 and 210.4 eV, corresponding to Nb $3d_{5/2}$ and Nb $3d_{3/2}$ spectra lines, respectively, which is characteristic of Nb^{5+}. These signals were slightly displaced at lower binding energies for mixed oxides, implying more Nb^{4+} and oxygen vacancies over the $Pt/Nb_2O_5/Al_2O_3$ systems. This behavior suggests the potential interaction of Pt species and Nb_2O_5. The lower shift in the binding energies observed for Pt $4f_{7/2}$ and Nb $3d_{5/2}$ in $Pt/Nb_2O_5/Al_2O_3$ systems when compared to Pt/Nb_2O_5 may result from the SMSI effect, due to the interactions formed between the Pt catalyst and Nb_2O_5. Recently, it has been reported that the SMSI can induce a reduction in the binding energy of Pt because of the direct interaction between the catalyst and oxide support [45].

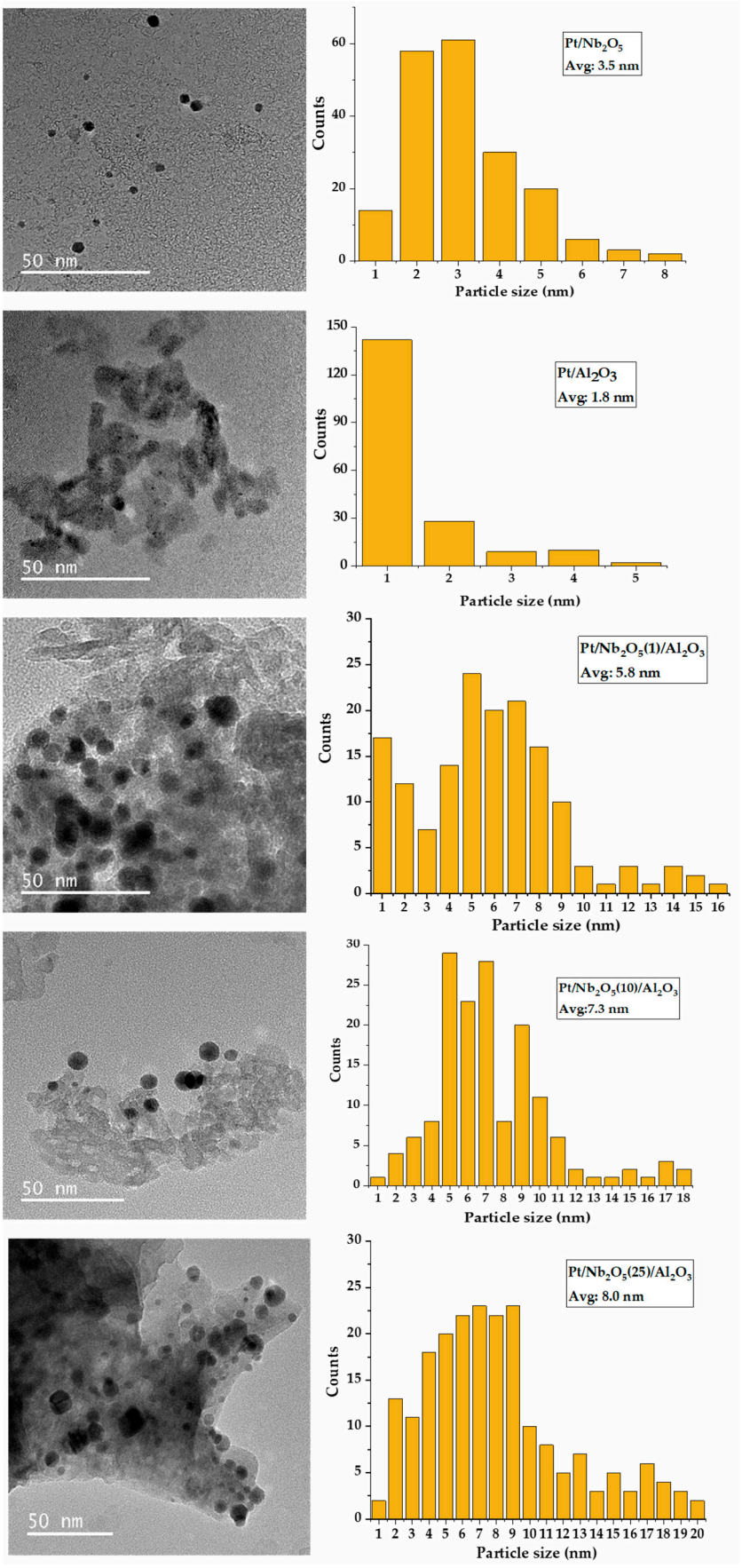

Figure 6. Typical TEM images and particle size distribution of passivated Pt catalysts.

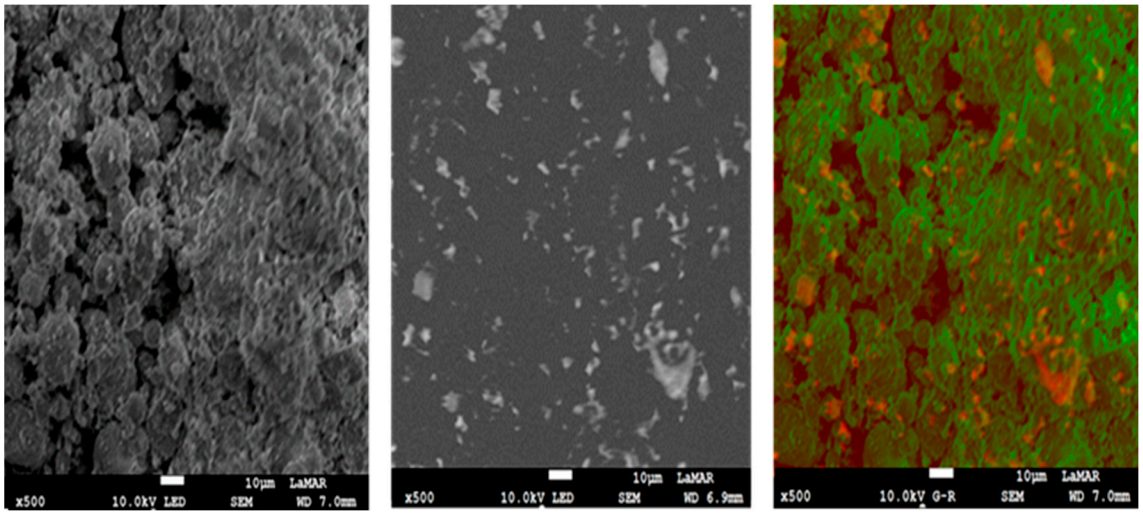

Figure 7. SEM images of $Pt/Nb_2O_5(25)/Al_2O_3$. Legend: orange corresponds to Nb and green corresponds to Al.

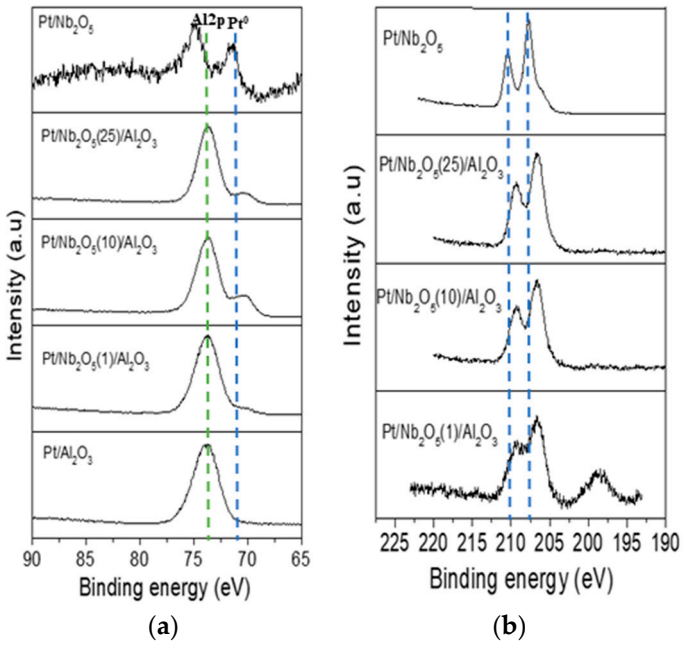

Figure 8. XPS spectra in (**a**) Pt 4f and (**b**) Nb 3d core level region of Pt catalysts supported.

In the case of $Pt/Nb_2O_5(1)/Al_2O_3$ there was a signal at 199 eV, which is generally ascribed to niobium-educed species. This behavior could be explained considering the well-known SMSI effect, assuming that NbO_x species migrate to metallic surfaces under the conditions of reduction employed. These results are consistent with the chemical states of Nb_2O_5 in previous reports [46,47]. This phenomenon occurs only at lowest proportions of Nb_2O_5 in the mixed oxides. It seems to be that a larger niobia content on the alumina surface is not able to migrate due to the strong Nb-O-Al interaction between both oxides. Moreover, the surface atomic ratio of Nb/Al reveals that an increase in Nb_2O_5 incorporation led to saturation of surface of alumina, causing a possible formation of niobia islands in mixed oxides.

2.2. Catalytic Activity

2.2.1. Furfural Hydrogenation

To calculate the initial activity, we applied polynomial differentiation at time zero to the furfural moles versus time curves. The initial TOF was calculated based on the initial activity, as described in the experimental section. Table 3 shows the results of initial activity and initial TOF. It can be seen that the most active catalyst was Pt/Nb_2O_5, while Pt/Al_2O_3 presented a lower conversion. Pt supported on mixed oxides does not show a trend marked with the niobia content increasing. However, it is clear that the incorporation of lower loadings of Nb_2O_5 ($Pt/Nb_2O_5(1)/Al_2O_3$) is similar to Pt/Nb_2O_5. The solid $Pt/Nb_2O_5(10)/Al_2O_3$ presented low activity compared with the other Pt catalysts supported on Nb_2O_5/Al_2O_3. This behavior could be explained considering the highest particle size of Pt when the solids contain Nb_2O_5; however, the atypical behavior of $Pt/Nb_2O_5(10)/Al_2O_3$ cannot be explained considering the particle size obtained. The evolution of the conversion and selectivity with time for the solids studied displays this same behavior (Figure 9).

Table 3. Results of initial activity and initial TOF for furfural hydrogenation.

Catalyst	$(-r)_0$ (μmol/s g cat)	TOF (s^{-1})
Pt/Al_2O_3	1.0	0.03
Pt/Nb_2O_5	7.0	0.37
$Pt/Nb_2O_5(1)/Al_2O_3$	7.0	0.25
$Pt/Nb_2O_5(10)/Al_2O_3$	4.5	0.15
$Pt/Nb_2O_5(25)/Al_2O_3$	5.7	0.25

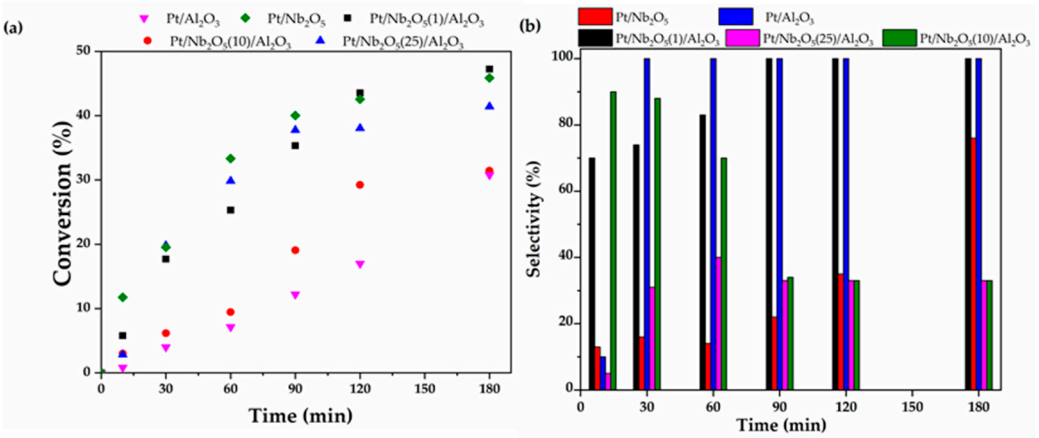

Figure 9. Evolution of the conversion of furfural (**a**) and selectivity to furfuryl alcohol (**b**) over Pt-supported catalysts.

With regard to selectivity to furfuryl alcohol, the catalysts showed notorious differences with respect to conversion. In the initial times, the more selective catalysts are those with a larger content of Al_2O_3, and, as the reaction progressed, the selectivity to furfuryl alcohol increased with the conversion, particularly for the $Pt/Nb_2O_5(1)/Al_2O_3$. Again, the $Pt/Nb_2O_5(10)/Al_2O_3$ displayed an anomalous behavior, as there was a decrease in the selectivity to furfuryl alcohol with time. Although the incorporation of niobia should increase the conversion, maintaining the selectivity of Pt/Al_2O_3, this only occurred at lower loadings of Nb_2O_5. Consequently, the highest incorporation of Nb_2O_5 showed a larger quantity of Pt^0 sites, causing the decrease in the selectivity to furfuryl alcohol. In addition, it can be seen that a larger particle size is not advantageous to obtain a higher conversion in the initial times, but assures a better adsorption via planar geometry through the C=C double bond of furfural.

As the reaction progresses, the preferential adsorption mode is sterically limited to vertical atop geometries through a C=O group favoring the formation of furfuryl alcohol. This condition in the mode of adsorption of furfural has been largely considered a decisive factor in the selectivity to unsaturated alcohol. In the case of $Pt/Nb_2O_5(10)/Al_2O_3$, the reaction toward alcohol takes place preferentially when the surface is not saturated, due to the larger fraction of metal exposed, as can be evidenced by XPS results. In general, the catalyst with the highest surface exposure of Pt species was not the most active, but the lowest Nb_2O_5 loading improved the conversion and selectivity of the Pt/Al_2O_3 catalyst. On the other hand, the presence of acid sites in Pt supported on mixed oxides leads to a detrimental effect of the selectivity to alcohol.

Table 4 shows the results of the spent catalysts, which was carried out to determine the stability of the catalysts. This process was carried out by recovering the solid through filtration after the reaction, then washing with deionized water and drying at 90 °C for 2 h. The reaction was carried out for 3 h, taking a sample at the beginning of the reaction (time 0, and a sample at the end time (3 h). The reaction conditions were the same as those used in the reaction for the determination of catalytic activity. As in the initial reaction to determine the catalytic activity of the synthesized solids, it will be observed that the catalyst that exhibited the best conversion was the $Pt/Nb_2O_5(1)/Al_2O_3$ catalyst and a yield of 96%. Likewise, it should be noted that the amount of catalyst used in reuse varied depending on the amount that was recovered from the initial reaction.

Table 4. Recyclability tests of the investigated catalysts under the following reaction conditions in the furfural hydrogenation: Pressure: 5 Mpa; temperature: 90 °C; speed: 1000 rpm; time: 3 h.

Catalyst	Furfural Conversion (%)		Selectivity Furfuryl Alcohol (%)	
	Run 1	Run 2	Run 1	Run 2
Pt/Al_2O_3	25	23	96	95
Pt/Nb_2O_5	42	40	72	70
$Pt/Nb_2O_5(1)/Al_2O_3$	43	42	79	66
$Pt/Nb_2O_5(10)/Al_2O_3$	28	25	30	26
$Pt/Nb_2O_5(25)/Al_2O_3$	37	35	30	28

2.2.2. Reductive Amination of Furfural

The reductive amination of furfural with aniline was chosen as a model reaction for reductive amination studies. The reductive amination of furfural involves, in the first step, the nucleophilic addition to the carbonyl group for the imine formation and the reduction of the imine group to give the amine as the second step. In consequence, the results of Table 5 summarize the data of conversion and yield to imine and yield to amine. It can be seen that the conversions in all solids are higher and similar due to the faster formation of imine, which occurs in the absence of catalyst. For this reason, we decided to express the results in yields to imine and amine. For Pt catalysts, the yield to imine is related to the acidic strength. Thus, the most acidic catalyst ($Pt/Nb_2O_5(25)/Al_2O_3$) showed the highest yield to imine.

Table 5. Results of conversion and yield to imine and amine at 8 h of reaction.

Catalyst	Conversion (%)	Y Imine (%)	Y Amine (%)
Blank	96	87	–
Pt/Al_2O_3	67	48	9
Pt/Nb_2O_5	82	47	18
$Pt/Nb_2O_5(1)/Al_2O_3$	80	40	19
$Pt/Nb_2O_5(10)/Al_2O_3$	82	40	23
$Pt/Nb_2O_5(25)/Al_2O_3$	89	59	14

The hydrogenation of imine is the rate-determining step of the reaction, and occurs more slowly. The yield to amine is highest for Pt catalysts containing Nb_2O_5, but an increase in acidity is not necessarily adequate to obtain a highest yield to amine. This can be rationalized as a highest adsorption of imine in the Lewis acid sites in this solid, which causes a minor hydrogenation of the C=N group. The presence of Lewis acid sites could favor the activation of the carbonyl group, making a better electrophile and consequently favoring the imine formation. A larger quantity of Lewis acid sites led to irreversible adsorption of the imine group.

The yield to amine as a function of the time of reaction is shown in Figure 10. The Pt/Nb_2O_5 catalyst displayed two-fold the yield to amine than Pt/Al_2O_3, but suffered a deactivation at 24 h. With regard to Pt supported on mixed oxides, the catalysts showed some interesting results; (i) the catalyst of higher niobia (25%) presents a lower yield than Pt/Nb_2O_5, (ii) a lower amount of Nb_2O_5 (1%) substantially increases the activity of Pt/Al_2O_3, maintaining the activity as the reaction progress, i.e., with a minor deactivation, (iii) the $Pt/Nb_2O_5(10)/Al_2O_3$ catalyst presents the highest yield to amine, probably as a consequence of a higher fraction of platinum exposed, as demonstrated by the XPS results. Thus, Pt catalysts deposited on Nb_2O_5 or Nb_2O_5/Al_2O_3 can exert a favorable effect over the yield to amine, probably associated with a larger particle size. However, a higher acidity could lead to irreversible adsorption of imine, causing a minor hydrogenation and consequently a lower yield to amine. On the other hand, this reaction, unlike furfural hydrogenation, is not dependent on the mode of adsorption of furfural, but it is totally independent of the metal-acidity function. The above results suggest that, in both reactions, the presence of reducible species (SMSI effect) and acid sites could favor the selectivity toward some interesting products in the hydrogenation and reductive amination reactions of furfural. Both conditions could be obtained using metal particles supported on reducible mixed oxides. A similar behavior was proposed by Wu et al. [48], when they synthesized a catalyst of Co_3O_4 supported on an advanced boron nitride nanosheet (BNNS) Co_3O_4/BNNS for methane oxidation. This system exhibited a high methane conversion rate, which was attributed to the formation of a BO_x over-layer confined Co_3O_4, ratifying the SMSI effect. Additionally, these results suggest that a tight interfacial contact is formed between Co_3O_4 and BNNS, which may help construct an interfacial confined environment and facilitate the interfacial charge transfer.

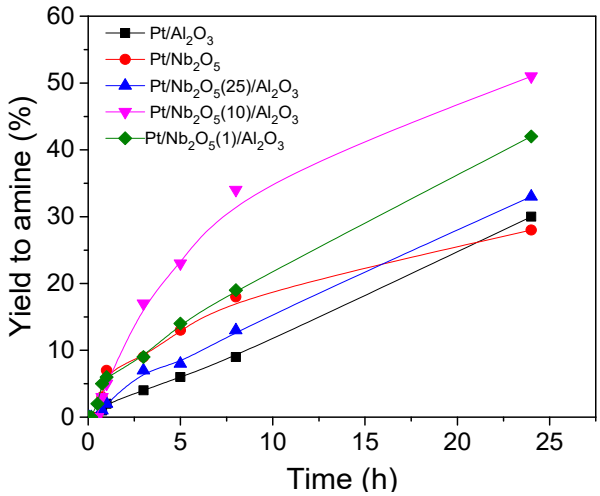

Figure 10. Yield to amine as function of the time of reductive amination of furfural.

Table 6 shows the comparison of $Pt/Nb_2O_5(1)/Al_2O_3$ catalyst as reported in the literature for the hydrogenation of furfural. The $Pt/Nb_2O_5(1)/Al_2O_3$ system exhibited high FOL selectivity (99%) and low FAL conversion at a short reaction time (3 h) compared with other catalysts. However, the Pt/Al_2O_3 catalysts tested in [49] showed a high conversion

and low selectivity at 5 h and 8 h of reaction, but the metal content was 5%. Table 7 shows the comparison of the performances of the $Pt/Nb_2O_5(10)/Al_2O_3$ in this research and the other catalysts reported in the furfural reductive amination. From the information, the $Pt/Nb_2O_5(10)/Al_2O_3$ system was found to have similar/comparable conversions and amine yields compared to those reported in the literature under mild conditions.

Table 6. Review of the hydrogenation of furfural to furfuryl alcohol on various supported Pt-based catalysts, and comparison of catalyst performance with literature data.

Catalysts	wt% Metal	Preparation Method	Reaction Conditions	Reaction Time (h)	FAL Conversion (%)	FOL Selectivity (%)	Ref.
$Pt/Nb_2O_5(1)/Al_2O_3$	1	Impregnation	90 °C, 25 mg, 5 MPa H_2	3 h	47	99	This work
Pt/TiO_2	0.5	Impregnation	50 °C, 50 mg, 20 bar H_2	2 h	89	17.7	[50]
Pt/AC	0.5	Impregnation	50 °C, 50 mg, 20 bar H_2	2 h	53.9	58	[51]
Pt/Al_2O_3	5.0	Wet impregnation	25 °C, 2 MPa H_2	8 h	30	99.1	[9]
Pt/Al_2O_3	5.0	Wet impregnation	240 °C, 2 MPa H_2	5 h	100	30.7	[9]
Pt/Al_2O_3	2.0	-	50 °C, Ambient	7 h	80	99	[52]
Pt/BC	3.0	Wet impregnation	210 °C, 10.3 MPa H_2	2 h	60.8	79.2	[49]
Pt/BC	3.0	Wet impregnation	180 °C, 1 MPa H_2	8 h	100	71	[53]
Nb_2O_5	-	Comercial	70 °C, 0.1 g, 20 bar H_2.	4 h	20	-	[54]

Table 7. Review of the reductive amination of furfural on various supported catalysts, and comparison of catalyst performance with literature data.

Catalysts	wt% Metal	Preparation Method	Reaction Conditions	Reaction Time	Conversion (%)	Amine Yield (%)	Ref.
$Pt/Nb_2O_5(10)/Al_2O_3$	1%	Impregnation	90 °C, 25 mg, 5 MPa H_2	8 h	82	33	This work
4Ru1Pt/AC	4Ru1Pt	Precipitation	100 °C, 50 mg, 2 MPa H_2,	2 h	99	33	[55]
$Au/SiO_2–SO_3H$	-	Precipitation	25 °C, 25 mg, 5 MPa H_2.	8 h	48	45	[23]
$Ir/SiO_2–SO_3H$	-	Precipitation	25 °C, 25 mg, 5 MPa H_2.	8 h	58	38	[23]
$Pt/SiO_2–SO_3H$	-	Precipitation	25 °C, 25 mg, 5 MPa H_2.	8 h	71	50	[23]
Ru/C	5%	Wet impregnation	100 °C, 0.15 g, 3 MPa H_2.	15 min	99	40	[22]
Ru/HZSM-5	5%	Wet impregnation	100 °C, 0.15 g, 3 MPa H_2.	15 min	99	76	[22]
Ru/S-1	5%	Wet impregnation	80 °C, 0.1 g, 2 MPa H_2.	2 h min	99	17	[22]
Blank	-	-	100 °C, 0.15 g, 3 MPa H_2.	15 min	99	<1	[22]
Pd/CNTs	1%	Wetness impregnation	120 °C, 50 mg	6 h	99	54	[56]
Pt/Al_2O_3	1%	Wetness impregnation	70 °C, 50 mg, 2 Mpa H_2.	24 h	100	18.9	[57]

3. Materials and Methods

3.1. Synthesis of Catalysts

Nb_2O_5/Al_2O_3 supports were prepared by wet impregnation of decaniobate salt $[N(CH_3)4]_6[Nb_{10}O_{28}]\cdot 6H_2O$ at distinct percentages over alpha-alumina powder. The solution was stirred for 3 h at 40°C, filtrated, and then the supports were dried at 120 °C and calcined at 550 °C for 4 h (10 °C/min) to obtain the Nb_2O_5/Al_2O_3 supports. Niobia loading were 0%, 1%, 10% and 20% (*w*/*w*). Alumina (SBA-200, Sasol, Johannesburg, South Africa) was previously calcined at 550 °C for 2 h with a heating rate of 10 °C/min. The decaniobate salt $[N(CH_3)_4]_6[Nb_{10}O_{28}]\cdot 6H_2O$ (HPNb) was synthesized according to the procedure reported by Ohlin et al. [58]. In a typical procedure, Nb_2O_5 (2.1 mmol) with an alcoholic solution of 3.3 mmol of tetramethylammonium hydroxide pentahydrate $[N(CH_3)_4]OH\cdot 5H_2O$ was heated to 120 °C in a Teflon-lined Parr vessel for 18 h, after which it was allowed to cool to room temperature and subsequently filtered, and the obtained solid was washed with acetone.

Pt/Nb_2O_5, Pt/Al_2O_3, and $Pt/Nb_2O_5/Al_2O_3$ catalysts were prepared by the conventional incipient wetness method (Pt loading = 1 wt%), using an aqueous solution of H_2PtCl_6 (Aldrich, 98%), followed by drying at 120 °C for 24 h and calcination treatment for 4 h at 500 °C, under 50 mL/min of synthetic air flow. Immediately before the catalytic test, the solid was reduced for 2 h at 500 °C under H_2 flow (30 mL/min). The catalysts were cooled in He flow and passivated at N_2 temperature using an O_2 (2%)/He mixture for 30 min.

3.1.1. Catalyst Characterization

The passivated solids were characterized by X-ray diffraction (XRD), Raman spectroscopy, N_2-physisorption at −196 °C, temperature-programmed desorption of ammonia (TPD-NH_3), adsorption of pyridine followed by diffuse reflectance infrared with Fourier transform spectroscopy (DRIFTS-Pyr), transmission electron microscopy analysis (TEM), H_2-chemisorption at room temperature, and X-ray photoelectron spectroscopy (XPS).

X-ray diffraction was carried out in a Rigaku diffractometer, using the powder method. The step size was 0.05° in the range of 2θ: 5°–90°. The adsorption–desorption of nitrogen isotherms was obtained at −196 °C. The samples were previously dried at 250 °C for 12 h and subsequently degassed at 120 °C for 2 h in-situ using Micromeritics ASAP 2020 equipment. The samples' surface area was calculated using the Brunauer–Emmett–Teller (BET) model, and the pore size distributions were calculated from the N_2 adsorption isotherm employing the Barrett–Joyner–Halenda (BJH) model.

H_2 chemisorption analyses were used to determine the dispersion of the active phase. The sample was dried at 150 °C, with a flow of He 30 (mL/min). Then, degassing was performed to ensure the elimination of any interference in the analysis. Once degassing was completed, the catalyst was reduced to 500 °C for 2 h and cleaned with He for 30 min at that temperature. It was then cooled to room temperature and the hydrogen adsorption isotherm was constructed. H_2 chemisorption experiments were carried out on Micromeritics ASAP 2020 equipment.

Raman spectroscopy measurements were carried out at room temperature using confocal Raman microscopy (Witec, alpha 300, Ulm, Germany), with a Nd-YAG green laser (532 nm) and 50× objective lens. All samples were analyzed with 500 scans.

Transmission electron microscopy (TEM) images were taken on a JEOL Model JEM-2100F microscope operated at an accelerating 200 kV voltage. Samples were prepared by dispersion in an ethanolic solution (50%) and sonicated for 1.5 h at room temperature. Subsequently, a drop of the suspension was applied on a copper grid (300 mesh). The particle size of the catalysts was calculated from the TEM images using Gatan digital microscopy software 3.

NH_3-temperature-programmed desorption was carried out in Micromeritics AutoChem 2920 equipment with a thermal conductivity detector (TCD). The samples were dried at 200 °C under Ar flow for 30 min and reduced at 500 °C for 2 h with H_2 flow (30 mL/min). Subsequently, the samples were cooled to 100 °C to carry out the adsorption of ammonia (30 mL/min) for 30 min, followed by cleaning with Ar flow at the same temperature to remove the physically adsorbed ammonia, and the temperature was decreased to 50 °C. The analysis started with the temperature increase up to 900 °C with a ramp of 10 °C/min, the NH_3 desorption profile of the analyzed sample was obtained.

Diffuse reflectance infrared with Fourier transform spectroscopy of pyridine (DRIFTS-Pyr) was carried out on a Nicolet iS50 equipment. The passivated catalysts were dried at 150 °C under He flow (15 mL/min) for 1 h, cooled to room temperature, and reduced to 400 °C under H_2 flow (30 mL/min) for 2 h. After reduction, the samples were purged with He (25 mL/min) for 30 min, cooled to room temperature, and a reference interferogram was taken at this temperature. Subsequently, pyridine (30 mL/min) was adsorbed for 1 h. After adsorption with pyridine, the catalyst was purged with He flow (20 mL/min) to eliminate the physisorbed pyridine, and then a new interferogram was taken at room temperature and related to the reference one, obtaining the spectrum of adsorbed pyridine.

X-ray photoelectron spectroscopy (XPS) analysis was performed with a Thermo Scientific ESCALAB 250 XI spectrometer. The studies were carried out with a pass energy of 25 eV, energy step of 0.05 eV, and dwell time of 50 ms. The pressure was kept around 10^{-8} mbar inside the analysis chamber. The spectra were calibrated employing the C 1s peak (284.6 eV). In the analysis of passivated samples, Ar^+ ion etching was used to break the oxygen film.

3.1.2. Catalytic Studies

Furfural hydrogenation and reductive amination were studied in a stainless-steel batch reactor at a constant stirring rate (1000 rpm) under the following conditions: hydrogen partial pressure, 5 MPa; catalyst sample, 25 mg; and reaction temperature of 90 °C. For the hydrogenation reactions, 40 mL of a 0.1 M solution of furfural in isopropanol was employed, while for the reductive amination, 40 mL of a 0.1 M solution of furfural and 0.1 M solution of aniline in ethyl acetate were employed. Reaction products of reductive amination of furfural were analyzed in a gas chromatographic coupled to a mass spectrometer (GC-MS Varian 3800) furnished with a β-Dex column, with He as the carrier, and a constant temperature of 120 °C. Both the products and the reactants of furfural hydrogenation were followed by a Knauer Azura high-efficiency liquid chromatograph (HPLC), equipped with a UV 1100 Azura lamp and a C18-type column. The conversion was determined with the following equation:

$$\text{Conversion}_{\text{FAL}}(\%) = \frac{\text{Initial mole of FAL} - \text{final mole of FAL}}{\text{Initial mole of FAL}} \times 100 \quad (1)$$

The selectivity to furfuryl alcohol was determined as follows:

$$\text{Selectivity}_{\text{FOL}}(\%) = \frac{\text{Mole of FOL}}{\sum \text{Mole of products}} \times 100 \quad (2)$$

The TOF was determined from the following equation:

$$\text{TOF}\left(\text{s}^{-1}\right) = \frac{(-\text{r}_\text{a})_0}{\text{Number of surface Pt atoms}} \quad (3)$$

where $(-\text{r}_\text{a})_0$ is the initial reaction rate. The number of surface Pt metal sites per mass loading of all catalysts was determined by hydrogen chemisorption.

4. Conclusions

The enrichment of Al_2O_3 with Nb_2O_5 in concentrations of 1 and 10% generated a decrease in the surface area, due to the possible obstruction of the pores of the Al_2O_3 by the Nb_2O_5. However, with the addition of 25% niobia, the surface area increased, possibly as a consequence of new mesoporosity. The dispersion of the active phase of the Pt/Al_2O_3-Nb_2O_5 catalysts decreased with increasing niobia content, and consequently, an increase in the average platinum particle size was observed. The results obtained in the acidity measurements for determination of both the strength of the acid sites and for the determination of their nature revealed that the catalysts presented acid sites of weak, intermediate, and strong strength, with both Lewis- and Brønsted-type sites, with the presence of Lewis sites being the most intense. Thus, the deposition of metal particles on mixed oxides is related to the niobia content and explains the results in the hydrogenation and reductive amination of furfural. A higher proportion of niobia islands led to better catalytic behavior in furfural hydrogenation due to the migration of reducible species, but a higher acidity could lead to irreversible adsorption of imine, causing a minor hydrogenation and consequently a lower yield to amine in the reductive amination of furfural.

Supplementary Materials: The following supporting information can be downloaded at: https://www.mdpi.com/article/10.3390/catal14080493/s1, Figure S1: Pore size distribution curve of the supported platinum catalysts; Figure S2: STEM-EDX image of the $Pt/Nb_2O_5(1)/Al_2O_3$ catalyst.

Author Contributions: M.H.B. contributed to formal analysis, conceptualization, methodology, software, investigation, supervision, data curation, and writing—review and editing; H.A.R. contributed to supervision and funding acquisition; J.J.M. contributed to resources, conceptualization, supervision, project administration, and funding acquisition; Y.X. contributed to methodology, software, and validation; F.B.P. contributed to conceptualization, supervision, data curation, writing—original draft

preparation, and writing—review and editing. All authors have read and agreed to the published version of the manuscript.

Funding: This research was funded by the Vicerrectoría de Investigación y Extensión–Universidad Pedagógica y Tecnológica de Colombia by the project SGI 3433.

Data Availability Statement: Data are contained within the article and Supplementary Files.

Acknowledgments: The authors acknowledge the financial support provided by the Vicerrectoría de Investigación y Extensión–Universidad Pedagógica y Tecnológica de Colombia by the project SGI 3433. FAPERJ and CNPq.

Conflicts of Interest: The authors declare no conflicts of interest.

References

1. Esteves, L.M.; Brijaldo, M.H.; Oliveira, E.G.; Martinez, J.J.; Rojas, H.; Caytuero, A.; Passos, F.B. Effect of support on selective 5-hydroxymethylfurfural hydrogenation towards 2, 5-dimethylfuran over copper catalysts. *Fuel* **2020**, *270*, 117524. [CrossRef]
2. Salnikova, K.; Matveeva, V.; Bykov, A.; Demidenko, G.; Shkileva, G.; Sulman, I. The Liquid Phase Catalytic Hydrogenation of the Furfural to Furfuryl Alcohol. *Chem. Eng. Trans.* **2018**, *70*, 379–384. [CrossRef]
3. Li, D.; Zhang, J.; Liu, Y.; Yuan, H.; Chen, Y. Boron doped magnetic catalysts for selective transfer hydrogenation of furfural into furfuryl alcohol. *Chem. Eng. Sci.* **2021**, *229*, 116075. [CrossRef]
4. Wang, Y.; Gao, T.; Lu, Y.; Wang, Y.; Cao, Q.; Fang, W. Efficient hydrogenation of furfural to furfuryl alcohol by magnetically recoverable RuCo bimetallic catalyst. *Green Energy Environ.* **2022**, *7*, 275–287. [CrossRef]
5. Gandarias, I.; García-Fernández, S.; Obregón, I.; Agirrezabal-Telleria, I.; Arias, P.L. Production of 2-methylfuran from biomass through an integrated biorefinery approach. *Fuel Process. Technol.* **2018**, *178*, 336–343. [CrossRef]
6. Rojas, H.; Martínez, J.J.; Reyes, P. Kinetic behavior in the hydrogenation of furfural over Ir catalysts supported on TiO_2. *DYNA* **2010**, *77*, 151–159.
7. Claus, P. Selective hydrogenation of α,β-unsaturated aldehydes and other C=O and C=C bonds containing compounds. *Top. Catal.* **1998**, *5*, 51–62. [CrossRef]
8. Villaverde, M.M.; Garetto, T.F.; Marchi, A.J. Liquid-phase transfer hydrogenation of furfural to furfuryl alcohol on Cu–Mg–Al catalysts. *Catal. Commun.* **2015**, *58*, 6–10. [CrossRef]
9. Bhogeswararao, S.; Srinivas, D. Catalytic conversion of furfural to industrial chemicals over supported Pt and Pd catalysts. *J. Catal.* **2015**, *327*, 65–77. [CrossRef]
10. Nguyen-Huy, C.; Lee, J.; Seo, J.H.; Yang, E.; Lee, J.; Choi, K.; Lee, H.; Kim, J.H.; Lee, M.S.; Joo, S.H.; et al. Structure-dependent catalytic properties of mesoporous cobalt oxides in furfural hydrogenation. *Appl. Catal. A Gen.* **2019**, *583*, 117125. [CrossRef]
11. Yuan, Q.; Zhang, D.; Van Haandel, L.; Ye, F.; Xue, T.; Hensen, E.J.M.; Guan, Y. Selective liquid phase hydrogenation of furfural to furfuryl alcohol by Ru/Zr-MOFs. *J. Mol. Catal. A Chem.* **2015**, *406*, 58–64. [CrossRef]
12. O'Driscoll, Á.; Leahy, J.J.; Curtin, T. The influence of metal selection on catalyst activity for the liquid phase hydrogenation of furfural to furfuryl alcohol. *Catal. Today* **2017**, *279*, 194–201. [CrossRef]
13. Delbecq, F.; Sautet, P. Competitive C=C and C=O Adsorption of α-β-Unsaturated Aldehydes on Pt and Pd Surfaces in Relation with the Selectivity of Hydrogenation Reactions: A Theoretical Approach. *J. Catal.* **1995**, *152*, 217–236. [CrossRef]
14. Pushkarev, V.; Musselwhite, N.; An, K.; Alayoglu, S.; Somorjai, G.A. High Structure Sensitivity of Vapor-Phase Furfural Decarbonylation/ Hydrogenation Reaction Network as a Function of Size and Shape of Pt Nanoparticles. *Nano Lett.* **2012**, *12*, 5196–5201. [CrossRef] [PubMed]
15. Jouve, A.; Cattaneo, S.; Delgado, D.; Scotti, N.; Evangelisti, C.; López Nieto, M.J.; Prati, L. Furfural Hydrogenation on Modified Niobia. *Appl. Sci.* **2019**, *9*, 2287. [CrossRef]
16. Du, H.; Ma, X.; Yan, P.; Jiang, M.; Zhao, Z.; Zhang, Z.C. Catalytic furfural hydrogenation to furfuryl alcohol over Cu/SiO_2 catalysts: A comparative study of the preparation methods. *Fuel Process. Technol.* **2019**, *193*, 221–231. [CrossRef]
17. Yang, X.; Meng, Q.; Ding, G.; Wang, Y.; Chen, H.; Zhu, Y.L.; Li, Y.W. Construction of novel $Cu/ZnO\text{-}Al_2O_3$ composites for furfural hydrogenation: The role of Al components. *Appl. Catal. A Gen.* **2018**, *561*, 78–86. [CrossRef]
18. Manikandan, M.; Venugopal, A.K.; Prabu, K.; Jha, R.K.; Thirumalaiswamy, R. Role of surface synergistic effect on the performance of Ni-based hydrotalcite catalyst for highly efficient hydrogenation of furfural. *J. Mol. Catal. A Chem.* **2016**, *417*, 153–162. [CrossRef]
19. Maderuelo-Solera, R.; López-Asensio, R.; Cecilia, J.A.; Jiménez-Gómez, C.P.; García-Sancho, C.; Moreno-Tost, R.; Maireles-Torres, P. Catalytic transfer hydrogenation of furfural to furfuryl alcohol over calcined MgFe hydrotalcites. *Appl. Clay Sci.* **2019**, *183*, 105351. [CrossRef]
20. Jackson, M.A.; White, M.G.; Haasch, R.T.; Peterson, S.C.; Blackburn, J.A. Hydrogenation of furfural at the dynamic Cu surface of $CuOCeO_2/Al_2O_3$ in a vapor phase packed bed reactor. *Mol. Catal.* **2018**, *445*, 124–132. [CrossRef]
21. Li, M.; Hao, Y.; Cárdenas-Lizana, F.; Keane, M.A. Selective production of furfuryl alcohol via gas phase hydrogenation of furfural over Au/Al_2O_3. *Catal. Commun.* **2015**, *69*, 119–122. [CrossRef]

22. Dong, C.; Wang, H.; Du, H.; Peng, J.; Cai, Y.; Guo, S.; Zhang, J.; Samart, C.; Ding, M. Ru/HZSM-5 as an efficient and recyclable catalyst for reductive amination of furfural to furfurylamine. *Mol. Catal.* **2020**, *482*, 110755. [CrossRef]
23. Martínez, J.J.; Nope, E.; Rojas, H.; Brijaldo, M.H.; Passos, F.; Romanelli, G. Reductive amination of furfural over Me/SiO_2-SO_3H (Me: Pt, Ir, Au) catalysts. *J. Mol. Catal. A Chem.* **2014**, *392*, 235–240. [CrossRef]
24. Reddy, P.S.; Kanjilal, S.; Sunitha, S.; Prasad, R.B.N. Reductive amination of carbonyl compounds using $NaBH_4$ in a Brønsted acidic ionic liquid. *Tetrahedron Lett.* **2007**, *48*, 8807–8810. [CrossRef]
25. Domine, M.E.; Hernández-Soto, M.C.; Navarro, M.T.; Pérez, Y. Pt and Pd nanoparticles supported on structured materials as catalysts for the selective reductive amination of carbonyl compounds. *Catal. Today* **2011**, *172*, 13–20. [CrossRef]
26. Bagal, D.B.; Watile, R.A.; Khedkar, M.V.; Dhake, K.P.; Bhanage, B.M. PS-Pd–NHC: An efficient and heterogeneous recyclable catalyst for direct reductive amination of carbonyl compounds with primary/secondary amines in aqueous medium. *Catal. Sci. Technol.* **2012**, *2*, 354–358. [CrossRef]
27. Chandra, D.; Inoue, Y.; Sasase, M.; Kitano, M.; Bhaumik, A.; Kamata, K.; Hosono, H.; Hara, M. A high performance catalyst of shape-specific ruthenium nanoparticles for production of primary amines by reductive amination of carbonyl compounds. *Chem. Sci.* **2018**, *9*, 5949–5956. [CrossRef] [PubMed]
28. Liu, Y.; Zhou, K.; Shu, H.; Liu, H.; Lou, J.; Guo, D.; Wei, Z.; Li, X. Switchable synthesis of furfurylamine and tetrahydrofurfurylamine from furfuryl alcohol over RANEY® nickel. *Catal. Sci. Technol.* **2017**, *7*, 4129–4135. [CrossRef]
29. Nakamura, Y.; Kon, K.; Touchy, A.S.; Shimizu, K.; Ueda, W. Selective Synthesis of Primary Amines by Reductive Amination of Ketones with Ammonia over Supported Pt catalysts. *ChemCatChem* **2015**, *7*, 921–924. [CrossRef]
30. Liang, G.; Wang, A.; Li, L.; Xu, G.; Yan, N.; Zhang, T. Production of Primary Amines by Reductive Amination of Biomass-Derived Aldehydes/Ketones. *Angew. Chem. Int. Ed.* **2017**, *56*, 3050–3054. [CrossRef] [PubMed]
31. Tran, S.B.T.; Choi, H.; Oh, S.; Park, J.Y. Influence of Support Acidity of Pt/Nb_2O_5 Catalysts on Selectivity of CO_2 Hydrogenation. *Catal. Lett.* **2019**, *149*, 2823–2835. [CrossRef]
32. Rodrigues, R.; Isoda, N.; Gonçalves, M.; Figueiredo, F.C.A.; Mandelli, D.; Carvalho, W.A. Effect of niobia and alumina as support for Pt catalysts in the hydrogenolysis of glycerol. *Chem. Eng. J.* **2012**, *198–199*, 457–467. [CrossRef]
33. Ma, L.; Yan, L.; Lu, A.-H.; Ding, Y. Effect of Re promoter on the structure and catalytic performance of Ni–Re/Al_2O_3 catalysts for the reductive amination of monoethanolamine. *RSC Adv.* **2018**, *8*, 8152–8163. [CrossRef] [PubMed]
34. Jiao, H.; Zhao, X.; Lv, C.; Wang, Y.; Yang, D.; Li, Z.; Yao, X. Nb_2O_5-γ-Al_2O_3 nanofibers as heterogeneous catalysts for efficient conversion of glucose to 5-hydroxymethylfurfural. *Sci. Rep.* **2016**, *6*, 34068. [CrossRef] [PubMed]
35. Gutierrez, L.F.; Nope, E.; Rojas, H.A.; Cubillos, J.A.; Sathicq, A.G.; Romanelli, G.P.; Martinez, J.J. New application of decaniobate salt as basic solid in the synthesis of 4H-pyrans by microwave assisted multicomponent reactions. *Res. Chem. Intermed.* **2018**, *44*, 5559–5568. [CrossRef]
36. Selvanathan, V.; Shahinuzzaman, M.; Selvanathan, S.; Sarkar, D.; Algethami, N.; Alkhammash, H.I.; Anuar, F.H.; Zainuddin, Z.; Aminuzzaman, M.; Abdullah, H.; et al. Phytochemical -Assisted Green Synthesis of Nickel Oxide Nanoparticles for Application as Electrocatalysts in Oxygen Evolution Reaction. *Catalysts* **2021**, *11*, 1523. [CrossRef]
37. Lima, S.; García-López, E.I.; Krivtsov, I.; Ilkaeva, M.; Bornes, C.; Mafra, L.; Liotta, L.F.; Villar-Rodil, S.; Paredes, J.I.; Marcì, G.; et al. Valorisation of microalga Chlorella sp. into furans in the presence of Nb_2O_5 catalysts. *J. Catal.* **2024**, *433*, 115457. [CrossRef]
38. Raba, A.M.; Bautista-Ruíz, J.; Joya, M. Synthesis and Structural Properties of Niobium Pentoxide Powders: A Comparative Study of the Growth Process. *Mater. Res.* **2016**, *19*, 1381–1387. [CrossRef]
39. Yang, D.; Huang, J.; Hu, Z.; Qin, S.; Mu, J.; Wang, F.; Zhang, Z.; Xie, Y.; Liu, S.; Wang, Q. Catalytic pyrolysis of lignin to aromatic hydrocarbons over Nb/Al oxide catalyst. *Energy* **2024**, *302*, 131764–131773. [CrossRef]
40. Kreissl, H.T.; Li, M.M.J.; Peng, Y.K.; Nakagawa, K.; Hooper, T.J.N.; Hanna, J.V.; Shepherd, A.; Wu, T.S.; Soo, L.Y.; Tsang, S.C.E. Structural Studies of Bulk to Nanosize Niobium Oxides with Correlation to Their Acidity. *J. Am. Chem. Soc.* **2017**, *139*, 12670–12680. [CrossRef] [PubMed]
41. Wachs, I.E. Raman and IR studies of surface metal oxide species on oxide supports: Supported metal oxide catalysts. *Catal. Today* **1996**, *27*, 437–455. [CrossRef]
42. González, G.; Saraiva, S.M.; Aliaga, W. Isoelectric points for niobium and vanadium pentoxides. *J. Dispers. Sci. Technol.* **1994**, *15*, 249. [CrossRef]
43. Gulicovski, J.J.; Čerović, L.S.; Milonjić, S.K. Point of zero charge and isoelectric point of alumina. *Mater. Manuf. Process.* **2008**, *23*, 615–619. [CrossRef]
44. Nascimento, J.P.; Oton, L.F.; Oliveira, A.C.; Rodríguez-Aguado, E.; Rodríguez-Castellón, E.; Araujo, R.S.; Souza, M.S.; Lang, R. Selective Catalytic Reduction of NO_x by CO over Doubly Promoted MeMo/Nb_2O_5 Catalysts (Me = Pt, Ni, or Co). *Catalysts* **2020**, *10*, 1048. [CrossRef]
45. Eckardt, M.; Gebauer, C.; Jusys, Z.; Wassner, M.; Hüsing, N.; Behm, R.J. Oxygen reduction reaction activity and long-term stability of platinum nanoparticles supported on titania and titania-carbon nanotube composites. *J. Power Sources* **2018**, *400*, 580–591. [CrossRef]
46. Lee, W.J.; Park, D.H.; Lee, H.J.; Byeon, J.H.; Kim, M.H.; Park, K.W. Enhanced oxygen reduction reaction performance of Pt catalysts on Nb_2O_5 nanoparticles decorated carbon nanostructures. *Mater. Sci. Eng. B* **2023**, *289*, 116253. [CrossRef]
47. Su, K.; Wang, Y.; Zhang, C.; Gao, Z.; Han, J.; Wang, F. Tuning the Pt species on Nb_2O_5 by support-induced modification in the photocatalytic transfer hydrogenation of phenylacetylene. *Appl. Catal. B Environ.* **2021**, *298*, 120554. [CrossRef]

48. Wu, H.; Sui, X.; Lei, Y.; Liu, L.; Xu, W.; Liang, G.; Li, C.; Li, X. Compositing of Co_3O_4 with boron nitride to promote the catalytic performance for methane oxidation. *Fuel* **2024**, *369*, 131786–131793. [CrossRef]
49. Fuente-Hernández, A.; Lee, R.; Béland, N.; Zamboni, I.; Lavoie, J.M. Reduction of Furfural to Furfuryl Alcohol in Liqui Phase over a Biochar-Supported Platinum Catalyst. *Energies* **2017**, *10*, 286. [CrossRef]
50. Kuhaudomlap, S.; Mekasuwandumrong, O.; Praserthdam, P.; Fujita, S.I.; Arai, M.; Panpranot, J. The H_2-Treated TiO_2 Supported Pt Catalysts Prepared by Strong Electrostatic Adsorption for Liquid-Phase Selective Hydrogenation. *Catalysts* **2018**, *8*, 87. [CrossRef]
51. Saknaphawuth, S.; Weerachawanasak, P.; Chuenchom, L.; Praserthdam, P.; Panpranot, J. Liquid-Phase Selective Hydrogenation of Furfural to Furfuryl Alcohol over Ferromagnetic Element (Fe, Co, Ni, Nd)-Promoted Pt Catalysts Supported on Activated Carbon. *Catalysts* **2022**, *12*, 393. [CrossRef]
52. Taylor, M.J.; Durndell, L.J.; Isaacs, M.A.; Parlett, C.M.A.; Wilson, K.; Lee, A.F.; Kyriakou, G. Highly selective hydrogenation of furfural over supported Pt nanoparticles under mild conditions. *Appl. Catal. B* **2016**, *180*, 580–585. [CrossRef]
53. Dohade, M.G.; Dhepe, P.L. One pot conversion of furfural to 2-methylfuran in the presence of PtCo bimetallic catalyst. *Clean Technol. Environ. Policy* **2017**, *20*, 703–713. [CrossRef]
54. Tian, Y.; Feng, Y.; Li, Z.; Fan, Y.; Sperry, J.; Sun, Y.; Yang, S.; Tang, X.; Lin, L.; Zeng, X. Green and efficient selective hydrogenation of furfural to furfuryl alcohol over hybrid CoO_x/Nb_2O_5 nanocatalyst in water. *Mol. Catal.* **2023**, *538*, 112981. [CrossRef]
55. Gou, L.; Xie, L.; Wang, Y.; Dai, L. Efficient conversion of furfural to furfural amine over 4Ru1Co/AC catalyst. *Appl. Catal. A* **2022**, *647*, 118902. [CrossRef]
56. Singh, G.; Kaishyop, J.; Singh, G.; Gazi, M.; Bag, A.; Samanta, C.; Bordolo, A. One-Pot direct reductive amination of furfural over Pd@CNTs. *Mol. Catal.* **2023**, *535*, 112877. [CrossRef]
57. Wang, H.; Zhang, Y.; Luo, D.; Wang, H.; He, Y.; Wang, F.; Wen, X. Active metal dependent side reactions for the reductive amination of furfural. *Mol. Catal.* **2023**, *536*, 112914. [CrossRef]
58. Ohlin, C.A.; Villa, E.M.; Casey, W.H. One-pot synthesis of the decaniobate salt $[N(CH_3)_4]_6[Nb_{10}O_{28}]\cdot 6H_2O$ from hydrous niobium oxide. *Inorg. Chim. Acta* **2009**, *362*, 1391–1392. [CrossRef]